

Massive post-starburst galaxies at $z > 1$ are compact proto-spheroids

Omar Almaini^{1*}, Vivienne Wild², David T. Maltby¹, William G. Hartley³,
Chris Simpson⁴, Nina A. Hatch¹, Ross J. McLure⁵, James S. Dunlop⁵, Kate Rowlands²

¹*School of Physics and Astronomy, University of Nottingham, University Park, Nottingham NG7 2RD, U.K.*

²*School of Physics and Astronomy, University of St Andrews, North Haugh, St Andrews, KY16 9SS, U.K.*

³*ETH Zürich, Institut für Astronomie, HIT J 11.3, Wolfgang-Pauli-Str. 27, 8093 Zürich, Switzerland*

⁴*Gemini Observatory, Northern Operations Center, 670 N. A'ohuku Place, Hilo, HI96720, USA*

⁵*Institute for Astronomy, University of Edinburgh, Royal Observatory, Blackford Hill, Edinburgh, EH9 3HJ, U.K.*

Accepted 2017 July 28. Received 2017 July 24; in original form 2016 February 3.

ABSTRACT

We investigate the relationship between the quenching of star formation and the structural transformation of massive galaxies, using a large sample of photometrically-selected post-starburst galaxies in the UKIDSS UDS field. We find that post-starburst galaxies at high-redshift ($z > 1$) show high Sérsic indices, significantly higher than those of active star-forming galaxies, but with a distribution that is indistinguishable from the old quiescent population. We conclude that the morphological transformation occurs before (or during) the quenching of star formation. Recently quenched galaxies are also the most compact; we find evidence that massive post-starburst galaxies ($M_* > 10^{10.5} M_\odot$) at high redshift ($z > 1$) are on average smaller than comparable quiescent galaxies at the same epoch. Our findings are consistent with a scenario in which massive passive galaxies are formed from three distinct phases: (1) gas-rich dissipative collapse to very high densities, forming the proto-spheroid; (2) rapid quenching of star formation, to create the “red nugget” with post-starburst features; (3) a gradual growth in size as the population ages, perhaps as a result of minor mergers.

Key words: galaxies: evolution – galaxies: formation – galaxies: fundamental parameters – galaxies: structure – galaxies: high-redshift

1 INTRODUCTION

Galaxies in the local Universe display a striking bimodality in their morphological and spectral characteristics; massive galaxies ($M_* > 10^{10.5} M_\odot$) are typically spheroidal with old stellar populations, while lower mass galaxies are typically disc-dominated with blue, younger stellar populations (e.g. Strateva et al. 2001; Hogg et al. 2002). Deep surveys have revealed that the most massive galaxies were formed at high redshift ($z > 1$; e.g. Fontana et al. 2004; Kodama et al. 2004; Cirasuolo et al. 2010), but we still do not understand why their star formation was abruptly terminated. Feedback from AGN (e.g. Silk & Rees 1998; Hopkins et al. 2005) or starburst-driven superwinds (e.g. Diamond-Stanic et al. 2012) are leading contenders for rapidly quenching distant galaxies, while jet-mode AGN feedback may be required to maintain the “red and dead” phase (e.g. Best et al. 2006).

In addition to the quenching of star formation, massive galaxies must also undergo a dramatic structural transformation, to produce the spheroid-dominated population we see today. The transition ap-

pears to occur at $z > 1$ for most galaxies with $M_* > 10^{10.5} M_\odot$ (Mortlock et al. 2013; Bruce et al. 2014), but it is unclear if quenching and structural transformation occurred during the same event. Over the last 10 years it has also emerged that quiescent galaxies were significantly more compact in the early Universe compared to the present day (e.g. Daddi et al. 2005; Trujillo et al. 2006; van Dokkum et al. 2008; Belli et al. 2014). Plausible explanations for the dramatic size growth include minor mergers (e.g. Bezanson et al. 2009; Naab, Johansson & Ostriker 2009) or expansion due to mass loss (Fan et al. 2008). For the population of quiescent galaxies as a whole, however, there may also be an element of progenitor bias; galaxies quenched at lower redshift tend to be larger than their counterparts at early times, which may drive much of the observed size evolution (e.g. Poggianti et al. 2013; Carollo et al. 2013).

From a theoretical perspective, the formation of ultra-compact massive spheroids requires the concentration of vast reservoirs of cool gas via dissipation, which can radiate and collapse to very high densities. A variety of models have arisen to explain spheroid formation in detail, with some invoking gas-rich mergers (e.g. Hopkins et al. 2009; Wellons et al. 2015) while others use the inflow of gas through cold streams, feeding an extended disc that eventually

* E-mail: omar.almaini@nottingham.ac.uk

becomes unstable and contracts (e.g. Dekel et al. 2009; Zolotov et al. 2015). Outflows driven by AGN or star formation may then terminate the star formation by expelling the remainder of the gas (e.g. Hopkins et al. 2005).

In this work we explore the relationship between the quenching of distant galaxies and their structural transformation. We focus in particular on the rare class of “post-starburst” (PSB) galaxies, which are observed a few hundred Myr after a major episode of star formation was rapidly quenched. In the local Universe PSBs are identified from characteristic strong Balmer absorption lines (Dressler & Gunn 1983; Wild et al. 2009), due to the strong contribution from A stars, but until recently very few were spectroscopically identified at $z > 1$ (e.g. Vergani et al. 2010). Two photometric methods have therefore been developed to identify this population. Whitaker et al. (2012) used medium-band photometry from the NEWFIRM Medium-Band Survey to identify “young red-sequence” galaxies using rest-frame UVJ colour-colour diagrams. In Wild et al. (2014) an alternative approach was used, based on a Principal Component Analysis (PCA) applied to the deep multi-wavelength photometry in the UDS field. Three spectral shape parameters (“supercolours”) were found to provide a compact representation for a wide range of photometric SEDs. In addition to cleanly separating quiescent and star-forming galaxies, the PCA method identifies “post-starburst” galaxy candidates in a distinct region of supercolour space, corresponding to galaxies in which a significant amount of mass was formed within the last Gyr but then rapidly quenched. The method was recently verified with deep 8m spectroscopy from VLT, which established that between 60% and 80% of photometric candidates are spectroscopically confirmed post-starburst galaxies, depending on the specific criteria adopted (Maltby et al. 2016)¹. In terms of completeness, the photometric method was found to identify approximately 60% of galaxies that would be spectroscopically classified as PSBs. Overall, these figures confirm that photometric PCA techniques can be used to identify large and relatively clean samples of recently quenched galaxies. So far the spectroscopic confirmation is restricted to $z < 1.4$, given the requirement to detect $H\delta$ with optical spectroscopy. Future near-infrared spectroscopy (e.g. with the *James Webb Space Telescope*) will allow a detailed investigation of the population at higher redshift.

The identification of large PSB samples has allowed the first study of the PSB galaxy mass function and its evolution to $z = 2$ (Wild et al. 2016). Strong evolution was observed, with the implication that a large fraction of massive galaxies are rapidly quenched and pass through a PSB phase. In this paper we use the unique PCA sample described in Wild et al. (2016) to explore the structural properties of post-starburst galaxies. As newly quenched systems, our primary aim is to investigate if this population is structurally similar to star-forming galaxies at the same epoch, or if they already show evidence for the compact spheroid-dominated morphology of well-established quiescent galaxies.

We assume a cosmology with $\Omega_M = 0.3$, $\Omega_\Lambda = 0.7$ and $h = 0.7$. All magnitudes are given in the AB system.

¹ From a sample of 24 PSB candidates, 19 galaxies (~80%) showed strong Balmer absorption lines ($W_{H\delta} > 5\text{\AA}$), dropping to 14 confirmations (~60%) if stricter criteria are used to exclude galaxies with significant [O II] emission. The fraction of spectroscopic PSBs among the passive and star-forming PCA classes was estimated to be <10% and <1% respectively (Maltby; private communication).

2 DATA AND SAMPLE SELECTION

2.1 The UDS K-band galaxy sample

Our study is based on deep K -band imaging from the UKIRT Infrared Deep Sky Survey (UKIDSS; Lawrence et al. 2007) Ultra-Deep Survey (UDS; Almaini et al. in prep). The UDS is the deepest of the UKIDSS surveys, covering 0.77 square degrees in the J , H and K bands. We use the 8th UDS data release (Hartley et al. 2013), reaching depths of $J = 24.9$, $H = 24.2$ and $K = 24.6$ (AB, 5σ , 2-arcsec apertures). The final UDS data release (June 2016) achieved estimated depths $J = 25.4$, $H = 24.8$, $K = 25.3$, and will be used to extend our PSB studies in future work.

To complement the near-infrared imaging from UKIDSS, the UDS has deep optical coverage from *Subaru* Suprime-CAM, to depths of $B = 27.6$, $V = 27.2$, $R = 27.0$, $i' = 27.0$ and $z' = 26.0$ (AB, 5σ , 2 arcsec), as described in Furusawa et al. (2008). Additional u' -band imaging is provided by the Canada-France-Hawaii Telescope (CFHT) MegaCam instrument, reaching $u' = 26.75$ (AB, 5σ , 2 arcsec). Deep imaging at longer near-infrared wavelengths is provided by the *Spitzer* UDS Legacy Program (SpUDS; PI: Dunlop), achieving depths of 24.2 and 24.0 (AB) using the IRAC camera at $3.6\mu\text{m}$ and $4.5\mu\text{m}$ respectively. The resulting area with full multiwavelength coverage, following the masking of bright stars and artefacts, is 0.62 square degrees. Further details on the construction of the multiwavelength DR8 catalogue can be found in Hartley et al. (2013).

We determined photometric redshifts using the techniques outlined in Simpson et al. (2013). The 11-band photometric data were fit using a grid of galaxy templates, assembled using simple stellar populations from Bruzual & Charlot (2003; hereafter BC03), with a logarithmic spacing of ages between 30 Myr and 10 Gyr, and the addition of younger templates with dust-reddened spectral energy distributions (SEDs). The additional templates consist of a mildly reddened ($A_V = 0.25$ mag) version of the two youngest templates, plus a version of the 30 Myr template with heavier reddening ($A_V = 1.0$ mag). The resulting photometric redshifts show a normalized median absolute deviation $\sigma_{\text{NMAD}} = 0.027$. The stellar masses used in this work differ slightly from those presented in Simpson et al. (2013), and instead are based on supercolour templates (see Section 2.3). As noted in Section 4.2, we investigated a range of alternative stellar masses, including those from Simpson et al. (2013), and found no significant impact on our conclusions.

2.2 Classification using PCA supercolours

We classify galaxies using a Principal Component Analysis (PCA) method applied to the broad-band photometric data, using the techniques outlined in Wild et al. (2014; hereafter W14). The aim of the PCA analysis is to describe the variation in galaxy SEDs using the linear combination of only a small number of components. The components are derived using a library of spectral synthesis models from BC03, using a wide range of stochastic star formation histories, metallicities, and dust-reddening. We found that only three principal components (effectively low-resolution “eigenspectra”) are required, in linear combination, to account for >99.9% of the variance in photometric SEDs. The amplitude of each component defines a “supercolour”, analogous to a traditional colour but defined using all available photometric bands. Supercolours allow the comparison of SEDs without the need for model fitting, and galaxies with extreme properties are free to have colours that differ substantially from any of the input model components.

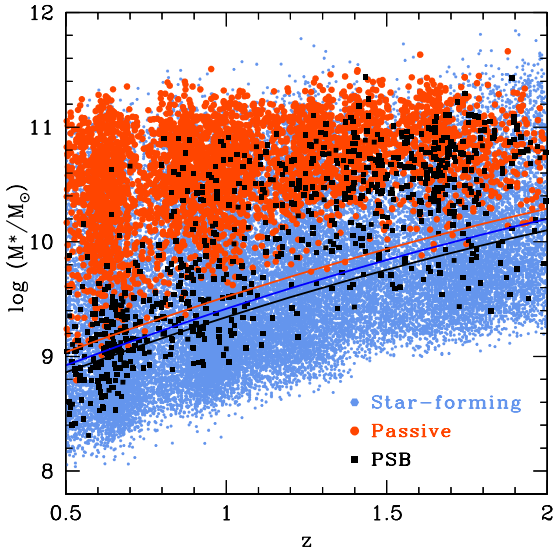


Figure 1. The distribution of stellar mass as a function of photometric redshift for the three primary galaxy populations. The curves show the corresponding 95% completeness limits, determined using the method of Pozzetti et al. (2010). Details of the galaxy classification and stellar mass determination can be found in Wild et al. (2016). In this paper we focus on the structural properties of galaxies in the redshift range $1 < z < 2$.

Using the supercolour technique, we separated the UDS galaxy population into three categories; passive galaxies (with low specific star-formation rates), star-forming galaxies, and post-starburst galaxies. Post-starburst galaxies are identified as a well-defined stream of galaxies in supercolour space, consistent with quiescent stellar populations in which a large fraction ($>10\%$) of the stellar mass was formed within the last ~ 1 Gyr, with the star formation then rapidly quenched (W14; see also Wild et al. 2016). The precise boundary between the passive and post-starburst population is set by the ability to observe strong Balmer absorption lines in optical spectroscopy (W14; Maltby et al. 2016). As outlined in Wild et al. (2016), evolutionary tracks suggest that not all photometric PSBs may have necessarily undergone a short-lived ‘burst’ of star formation. The population may also include galaxies that have undergone more extended ($\lesssim 3$ Gyr) periods of star formation, but the key characteristic is the rapid quenching of star formation within the last ~ 1 Gyr.

In W14, four categories of star-forming galaxies were identified (SF1, SF2, SF3 and dusty), which we combine for the purposes of this work. As outlined in W14 (see also Section 4.3) the classification by supercolours is in very good agreement with the separation of galaxies using the more traditional rest-frame UVJ technique for separating star-forming and passive galaxies (Labbé et al. 2005; Wuyts et al. 2007). There is also good agreement with the UVJ method of Whitaker et al. (2012), who identified recently-quenched candidates at the blue end of the passive UVJ sequence.

2.3 Stellar masses

We determined stellar masses for each galaxy using a Bayesian analysis, to account for the degeneracy between physical parameters. Further details may be found in Wild et al. (2016). A library of 10’s of thousands of population synthesis models was created using BC03 and fit to the supercolours to obtain a probability density

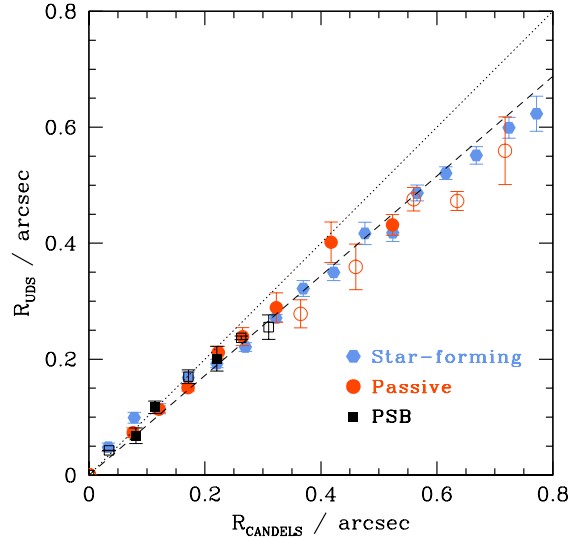
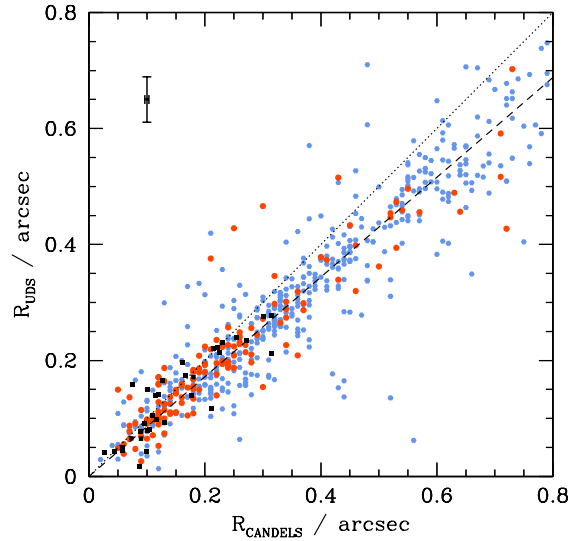


Figure 2. A comparison of size measurements for galaxies measured with ground-based K -band imaging and HST H -band imaging, using the subsample of $\sim 9\%$ of galaxies within the UDS CANDELS mosaic. The upper panel compares half-light radii for individual galaxies. We find that ground-based imaging can provide robust measurements of galaxy sizes, although the relationship is not precisely 1:1. A linear fit to all points suggests that ground-based sizes are $\sim 13\%$ smaller on average (dashed line). A characteristic uncertainty on individual measurements is shown, representing the median error on the PSB sizes. The lower (binned) distribution compares mean sizes for the three key populations, with unfilled symbols representing mean values determined from fewer than 5 galaxies. We find no evidence for a significant systematic bias in ground-based size determinations with spectral type. Galaxies shown have photometric redshifts in the range $1 < z < 2$ and stellar masses with $\log(M_*/M_\odot) > 10$, to match the samples used in this work.

function for each physical property. A wide range of star formation histories, dust properties, and metallicities were explored, including exponentially declining star formation rates with superimposed stochastic starbursts. Stellar masses were calculated assuming a Chabrier initial mass function (IMF), defined as the stellar mass at the time of observation, i.e. allowing for the fraction of mass in

stars returned to the interstellar medium due to mass loss and supernovae. The resulting stellar mass uncertainties from the Bayesian fits are typically ± 0.1 dex for all populations, assuming BC03 stellar population synthesis models and allowing for uncertainties in the photometric redshifts. The potential impact of stellar mass errors (random and systematic) is discussed further in Section 4.2.

Figure 1 shows the resulting distribution of stellar mass as a function of redshift, separated into the three primary populations. Mass completeness limits (95%) were determined as a function of redshift using the method of Pozzetti et al. (2010). We note that the 95% completeness limit for star-forming galaxies appears to be surprisingly high in this diagram (formally slightly higher than the PSB population). This is caused by the wide range in mass-to-light ratios within the star-forming population.

As outlined in Wild et al. (2016), the PSB mass function evolves strongly with redshift, so that the comoving space density of massive PSBs ($M_* > 10^{10} M_\odot$) is several times higher at $z \sim 2$ than at $z \sim 0.5$. This trend is apparent in Figure 1, which shows a sharp decline in the number of massive PSBs at $z < 1$. The majority of PSBs at $z < 1$ are close to the 95% completeness limit (see Figure 1) and typically very faint; the median K -band magnitude for PSBs at $z < 1$ is $K = 23.0$, compared to $K = 21.8$ at $z > 1$. In this work we therefore concentrate on the structural properties of PSBs at $z > 1$, and defer an examination of the low-redshift ground-based sample to future work using deeper K -band imaging. In the redshift range $1 < z < 2$, our initial sample consists of 24,880 star-forming galaxies, 2043 passive galaxies and 502 PSBs, of which 9183, 2001 and 385, respectively, have stellar masses $M_* > 10^{10} M_\odot$.

2.4 CANDELS-UDS

Throughout this work we compare our ground-based determinations of galaxy size and Sérsic index with measurements from the Hubble Space Telescope (HST) CANDELS survey (Grogin et al. 2011; Koekemoer et al. 2011), using measurements provided in van der Wel et al. (2012). The UDS is one of the three targets for the CANDELS Wide survey, with imaging in the J and H bands taken with the Wide Field Camera 3 (WFC3). The CANDELS imaging covers only $\sim 7\%$ of the UDS field ($\sim 9\%$ of the area used in our analysis), but this is sufficient to provide an independent test and calibration for our ground-based structural parameters. Full details of the GALFIT measurement of structural parameters within CANDELS are given in van der Wel et al. (2012).

3 GROUND-BASED MEASUREMENTS OF SIZE AND SÉRSIC INDEX

We determined structural parameters for the K -band galaxy sample using the GALAPAGOS software (Barden et al. 2012). The package allows the automated use of GALFIT (Peng et al. 2002) to fit Sérsic light profiles (Sérsic 1968) to all galaxies in the UDS, parameterized with a Sérsic index, n , and effective radius, R_e , measured along the semi-major axis. We acknowledge that many high-redshift galaxies are described by more complex morphologies (see Bruce et al. 2014), but single Sérsic fits provide a simple parameterization to allow us to compare the bulk properties of the galaxy populations.

An accurate determination of the point-spread function (PSF) is critical for this process, as galaxies at $z > 1$ typically have half-light radii below 0.5 arcsec. Following the work of Lani et al. (2013), we investigated PSF variations across the UDS field and found that most variation occurred between WFCAM detector boundaries

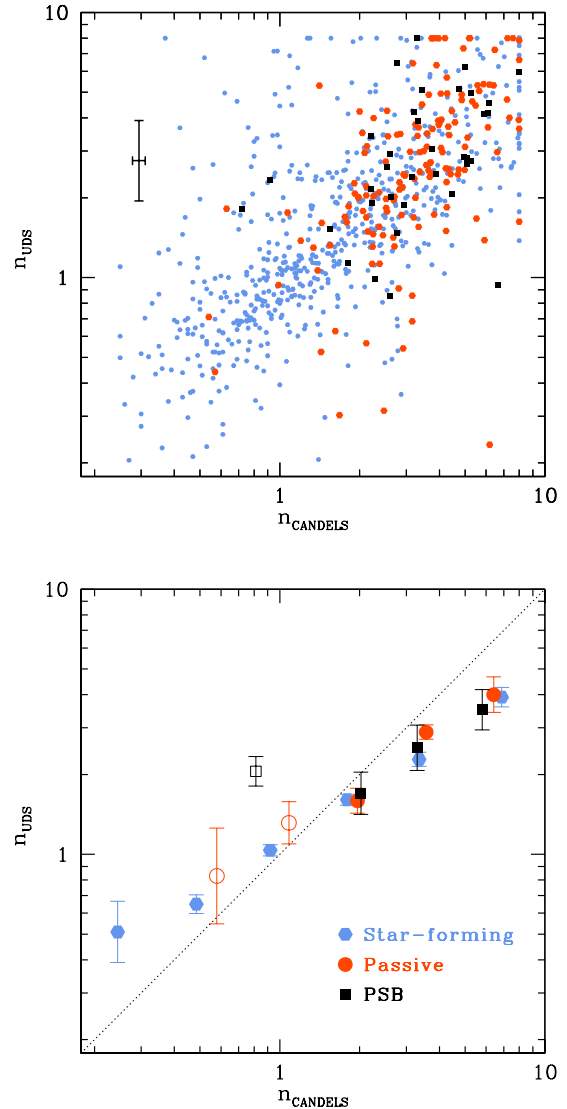


Figure 3. A comparison of Sérsic index measurements for galaxies measured with ground-based K -band imaging and HST H -band imaging, using the subsample of $\sim 9\%$ of galaxies within the UDS CANDELS mosaic. The upper panel compares individual galaxies, with a characteristic error bar denoting the median uncertainty in $\log_{10}(n)$ for the PSB population. We find that ground-based determinations of Sérsic indices are sufficient to broadly distinguish populations with high average values from those with low average values. The lower (binned) distribution compares the mean Sérsic indices, binned as a function of n_{CANDELS} . Open symbols denote mean values determined from fewer than 5 galaxies. There are deviations from a 1:1 relation, but no evidence for a systematic bias in ground-based Sérsic determinations with spectral type. Galaxies shown have photometric redshifts in the range $1 < z < 2$ and stellar masses with $\log(M_*/M_\odot) > 10$, to match the samples used in this work.

within the UDS mosaic (Casali et al. 2007). Testing revealed that we could obtain consistent results by splitting the UDS field into 16 overlapping sub-regions, corresponding to the 4×4 WFCAM tiling pattern. Within each region the light profiles of approximately 100 stars were stacked to provide the local PSF measurement, with variations across the field in the range 0.75 – 0.81 arcsec (FWHM).

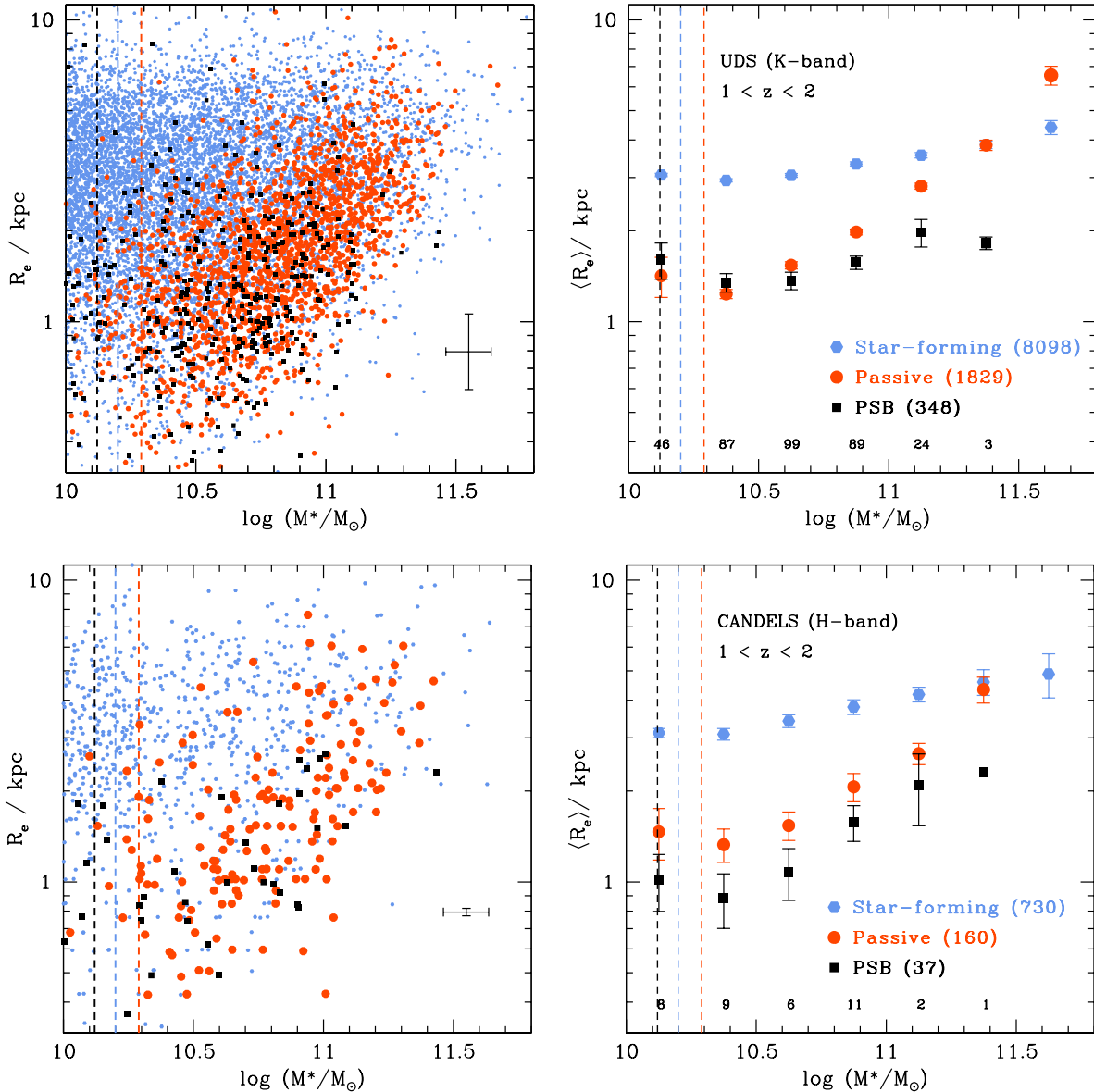


Figure 4. The stellar size-mass relation for star-forming, passive and post-starburst galaxies in the redshift range $1 < z < 2$. The top figures show the results from the ground-based K -band sample, showing individual galaxies (left) and mean sizes as a function of stellar mass (right). For the individual galaxies (left), a characteristic 1σ error bound is displayed, showing the median uncertainties in the fitted size and stellar mass for the post-starburst population. For the binned relation (right), the numbers in parentheses denote the number of galaxies in each sample, while the number of PSBs per mass bin is also shown. Errors on mean sizes represent the standard error on the mean (though we caution that the highest mass PSB bin contains only 3 galaxies). The lower figures show the equivalent for the subsample of galaxies with HST CANDELS H -band imaging, with sizes determined by van der Wel et al. (2012). Very similar trends are observed, although we note the small sample of PSBs (e.g. one galaxy in the highest mass bin). Overall, we conclude that post-starburst galaxies are exceptionally compact, with evidence that (on average) they are smaller than typical quiescent galaxies at the highest stellar masses ($M_* > 10^{10.5} M_\odot$). The dashed vertical lines denote the 95% completeness limits, determined at the upper redshift range ($z = 2$).

Considerable care was taken to mask sources in the vicinity of the stars used for PSF measurement.

From the resulting measurements of size and Sérsic index we rejected $\sim 9\%$ of galaxies where GALFIT failed to converge on a Sérsic solution. The rejection rate was similar for the star-forming, passive and post-starburst populations. A further $\sim 1\%$ of galaxies were rejected (a-priori) if the fits were formally very poor ($\chi^2_\nu > 100$), which typically corresponded to highly blended objects on the K -band image. Matching the output from GALAPAGOS with our Supercolour catalogue, we obtain a final sample of 8098

star-forming galaxies, 1829 passive galaxies, and 348 PSBs in the redshift range $1 < z < 2$ with $M_* > 10^{10} M_\odot$.

In Figures 2 and 3 we display the resulting size and Sérsic measurements for the subset of UDS galaxies within the HST CANDELS survey. Ground-based measurements are compared with those obtained using H -band CANDELS measurements, as published in van der Wel et al. (2012).

For the size measurements, we find a tight relationship between the ground-based K -band and CANDELS H -band sizes, as previously found by Lani et al. (2013). On average, the sizes ob-

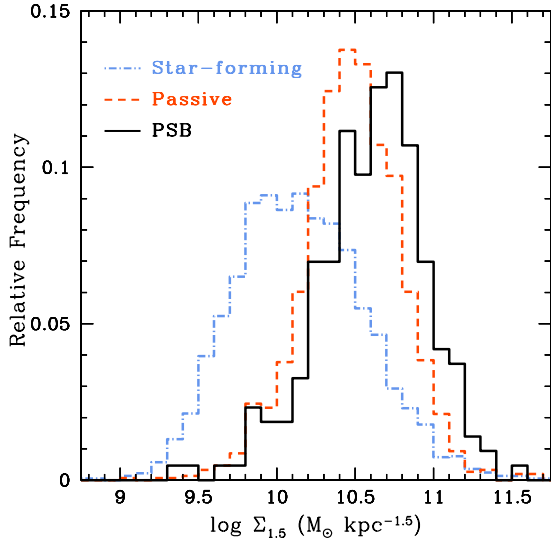


Figure 5. We compare the distribution of $\Sigma_{1.5}$ values for the three galaxy populations in the redshift range $1 < z < 2$, with stellar masses $M_* > 10^{10.5} M_\odot$. This parameter ($\Sigma_{1.5} \equiv M_*/R_e^{1.5}$), defined by Barro et al. (2013), effectively removes the slope of the galaxy mass/size relation; high values of $\Sigma_{1.5}$ correspond to galaxies that are compact for their stellar mass. A KS test rejects the null hypothesis that passive galaxies and PSBs are drawn from the same underlying distribution in $\Sigma_{1.5}$, with a significance of $> 99.99\%$.

tained from CANDELS are systematically $\sim 13\%$ larger, which is consistent with previous comparisons of size measurements as a function of waveband (e.g. Kelvin et al. 2012). The systematic offset is consistent among the three galaxy populations studied here so we apply no corrections for this effect. The characteristic scatter in $\delta R/R$, given by the normalized median absolute deviation (σ_{NMAD}) is 17%, 16% and 24% for the star-forming, passive and PSB populations respectively.

Ground-based measurements of Sérsic index are far more uncertain for a given galaxy (Figure 3), and we find a significant degree of scatter when comparing ground-based and CANDELS measurements. Formally, the characteristic scatter in $\delta n/n$, given by the normalized median absolute deviation (σ_{NMAD}) is 45%, 39%, and 35% for the star-forming, passive and PSB populations respectively. Nevertheless, there is a clear correlation, and we find that ground-based determinations are sufficient to distinguish populations with “high” Sérsic indices (e.g. $n > 2$) from those with “low” Sérsic indices ($n < 2$). Comparing the three primary galaxy types, we find consistent results; the passive and post-starburst populations show consistently high Sérsic indices (from ground or space-based measurements), while star-forming galaxies are concentrated at lower values. The binned distribution demonstrates that the correlation between ground and space-based Sérsic indices is not perfectly 1:1, but we see no systematic differences in this relation between the three populations. We conclude that ground-based measurements can be used to broadly compare the Sérsic indices for our galaxy populations. In addition, we will use the subset of galaxies with HST measurements ($\sim 9\%$) to verify any conclusions drawn from the larger ground-based sample. The Sérsic distributions will be compared further (and as a function of stellar mass) in Section 5.

4 THE SIZES OF POST-STARBURST GALAXIES

4.1 The size–mass relation

In Figure 4 we compare the size versus stellar-mass relation for galaxies in the redshift range $1 < z < 2$. Individual galaxies are shown, along with mean values as a function of stellar mass (in bins of 0.25 dex). In the upper panels we show the results from the ground-based K -band imaging, while the lower panels are based on independent sizes from CANDELS H -band imaging (covering $\sim 9\%$ of the sample). The 95% mass completeness limits are shown (see Section 2.3), determined at $z = 2$ to provide conservative limits. In determining mean values for the ground-based sample we applied a 5σ clip (with one iteration), to remove extreme outliers, but removing this constraint has no significant influence.

Representative error bounds for individual galaxies are shown on the left panels, based on the median errors on the PSB sample. For the CANDELS sizes, data are taken from van der Wel et al. (2012), which include estimates for random and systematic errors from GALFIT. For the ground-based individual errors, we add in quadrature the scatter in $\delta R/R$ determined by the comparison with CANDELS (Section 3). The representative uncertainty on stellar masses is based on our Bayesian mass-fitting analysis described in Wild et al. (2016), as briefly outlined in Section 2.3.

The size–mass relations show the expected trends for star-forming and passive galaxies, consistent with previous studies (e.g. Daddi et al. 2005; Trujillo et al. 2006; van Dokkum et al. 2008; van der Wel et al. 2014; McLure et al. 2013). On average, passive galaxies appear significantly more compact than star-forming galaxies of equivalent stellar mass, but show a steeper size–mass relation, leading to convergence at the highest masses ($M_* \sim 10^{11.5} M_\odot$). Intriguingly, we find that post-starburst galaxies at this epoch are also extremely compact; they are comparable in size to the established passive galaxies, with evidence that they are smaller on average at high mass ($M_* > 10^{10.5} M_\odot$). These trends are apparent with the large ground-based sample and with the smaller CANDELS sample.

We performed a bootstrap analysis as a simple test of significance, randomly sampling the (ground-based) populations within each mass bin, with replacement. For the 4 bins above $10^{10.5} M_\odot$, the fraction of the resampled populations in which the passive galaxies show mean sizes equal to (or smaller than) the mean of the PSB population are 0.07, 5×10^{-5} , 1.2×10^{-4} , 4×10^{-5} (low to high mass, respectively). We note that the final bin contains 86 passive galaxies, but only 3 PSBs, so the bootstrap comparison for this bin may be unreliable. Overall, assuming no systematic errors, we find evidence that massive post-starburst galaxies at $z > 1$ are significantly more compact, on average, than passive galaxies of comparable mass. Repeating the analysis using the median sizes produced very similar trends. The median analysis and further tests of robustness are presented in Appendix A. Our results are consistent with the findings of Yano et al. (2016), who also found evidence that high-redshift post-starburst galaxies are very compact.

As an additional comparison, in Figure 5 we display the distribution of $\Sigma_{1.5} \equiv M_*/R_e^{1.5}$ for the three galaxy populations, measured for the redshift range $1 < z < 2$ and stellar masses $M_* > 10^{10.5} M_\odot$. Following Barro et al. (2013), we use this parameter to effectively remove the slope in the galaxy size/mass relation. Fitting a function of the form $M_* = \Sigma R_e^\alpha$ to the passive population, we find a best fit with $\alpha = 1.55$, in very good agreement with the value $\alpha = 1.5$ assumed by Barro et al. (2013). A simple Kolmogorov-Smirnov (KS) test rejects the null hypothesis that passive galaxies and PSBs are drawn from the same underlying

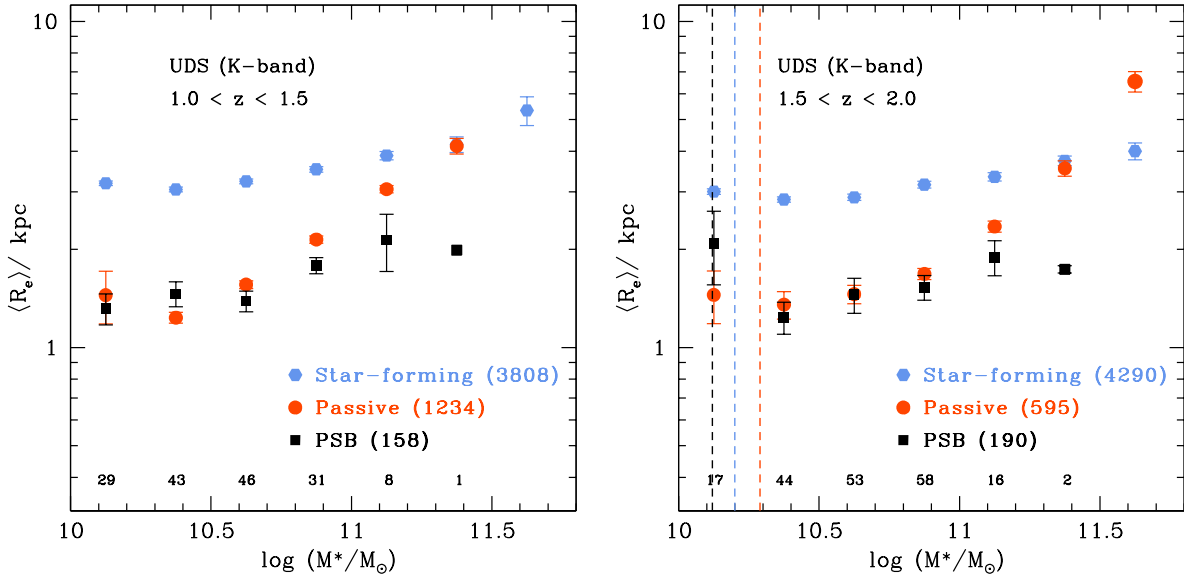


Figure 6. A comparison of the galaxy mean size–stellar mass relation for star-forming, passive and post-starburst galaxies in two redshift bins. The numbers in parentheses denote the number of galaxies in each sample, while the number of PSBs per mass bin is shown at the bottom of each plot. Errors on mean sizes represent the standard error on the mean (though we note the small number of PSBs in the highest mass bins). The vertical lines denote the 95% completeness limits (all below $10^{10} M_\odot$ for the low-redshift bin).

distribution in $\Sigma_{1.5}$ with a significance $> 99.99\%$, with the same significance obtained with either value of α .

Given the strong evolution of the PSB mass function (Wild et al. 2016), a concern is that massive PSBs are more common at higher redshifts, which may bias the size–mass comparison when measured over a wide redshift range. In Figure 6 we therefore display the size–mass relation in two narrower redshift bins, $1.0 < z < 1.5$ and $1.5 < z < 2.0$. With two independent samples, the results confirm that post-starburst galaxies, on average, show smaller half-light radii than the passive population at high mass ($M_* > 10^{10.5} M_\odot$). An additional test was performed using a weighted mean, with a redshift-dependent weight determined for each PSB using the ratio of the $n(z)$ distributions for passive galaxies and PSBs. The resulting size–mass relations were barely changed, with only a slight reduction in the significance of the differences reported above.

A natural interpretation of our findings is that quiescent galaxies are most compact when they are newly-quenched, but then grow with cosmic time. Given the short-lived nature of the PSB phase, we expect the majority of passive galaxies to have gone through a similar stage in their past (Wild et al. 2016). Our results therefore provide evidence for the genuine growth of individual galaxies, suggesting that the growth of the population as a whole is not purely caused by a progenitor bias. We discuss the implications further in Section 6.

A simple calculation allows us to compare the size differences with the observed cosmological growth. Based on population synthesis models, we estimate that the established passive population quenched approximately 0.5–1 Gyr before the PSB population at these redshifts (Wild et al. 2016), and the characteristic difference in size (e.g. based on the shift in $\Sigma_{1.5}$) is approximately 25% on average at $M_* > 10^{10.5} M_\odot$. The implied growth rate is similar to the observed *cosmological* growth, parameterized by van Dokkum et al. (2010) in the form $r_e \propto (1+z)^{-1.3}$ (i.e. $\sim 25\%$ per Gyr at $z = 1.5 - 2$). An improvement on these tentative conclusions will

require more accurate age-dating of the stellar populations, which will soon be possible with growing spectroscopic samples.

4.2 Stellar mass uncertainties

In this section we explore the potential impact of both random and systematic errors on our stellar masses.

The typical uncertainty from our Bayesian stellar mass fitting is $\sigma \simeq 0.1$ dex for all galaxy types, allowing for the degeneracy between fitted parameters and the uncertainties on photometric redshifts. To investigate the impact on our conclusions, we performed Monte Carlo realisations, allowing the stellar masses to shift randomly within a Gaussian probability distribution in $\log M_*$. We found no impact on any of the results presented in Section 4.1. Comparing the resulting distributions in $\Sigma_{1.5}$, the significance of the difference between the PSB and passive galaxy populations was unchanged, suggesting that the sample overall is large enough to minimise the influence of random errors.

To investigate the influence of fitting methods, we re-evaluated the size–mass relations using two independent sets of stellar masses derived by Simpson et al. (2013) and Hartley et al. (2013), the latter also using an independent set of photometric redshifts. No significant differences were found.

As a note of caution, however, we acknowledge that the observed differences between PSBs and passive galaxies could arise if our stellar masses are *systematically* overestimated for younger stellar populations. Our stellar masses are based on population synthesis models from BC03, which may underestimate the influence of thermally-pulsing asymptotic giant branch (TP-AGB) stars (Maraston et al. 2006). Such stars may have a major contribution to the rest-frame near-infrared light for stellar populations in the age range 0.2 to 2 Gyr, potentially leading to overestimated stellar masses for passive galaxy populations. The influence of TP-AGB stars is discussed further in Wild et al. (2016), where it was found that the influence of TP-AGB stars is strongest for galaxies with BC03-

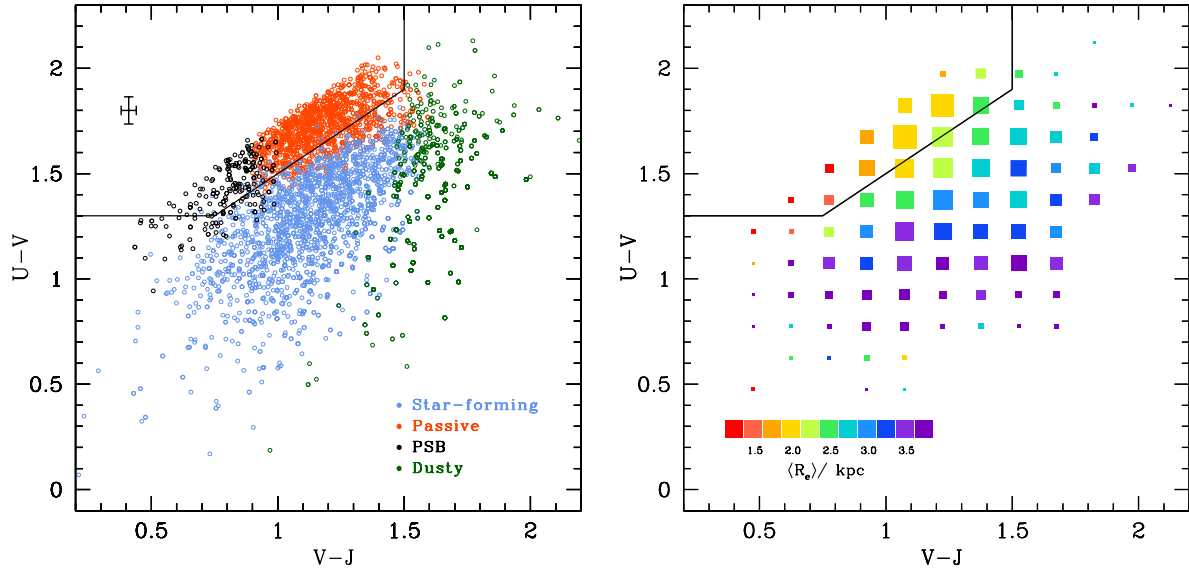


Figure 7. Rest-frame UVJ colour-colour diagrams for UDS galaxies in the redshift range $1 < z < 2$, and within the mass range $10.5 < \log (M_*/M_\odot) < 11.5$. Previous studies have separated galaxies into “quiescent” and “star-forming” categories using the boundary shown. The left panel compares the classification of galaxies using supercolours with the UVJ method (in this diagram separating the dusty PCA class from the other star-forming galaxies). We find good agreement between the classification methods, with a very similar boundary between star-forming and passive types. Post-starburst galaxies selected by supercolours are primarily located at the blue end of the quiescent UVJ region, in good agreement with the boundaries proposed by Whitaker et al. (2012). A representative error bar is displayed, showing the median uncertainties for the PSB population. The right-hand panel shows average sizes determined for all galaxies in colour-colour bins, without using supercolours. Symbol size is proportional to the number of galaxies per bin. The trends confirm that “young-quiescent” galaxies selected by the UVJ technique show smaller average sizes than redder passive galaxies, consistent with our classification based on PCA supercolours.

determined ages > 1 Gyr, for which the ages and mass-to-light ratios are reduced using the models of Maraston et al. (2006). The net effect would be to move our passive galaxies to lower masses relative to the younger PSB population, which would *enhance* the differences in the size–mass relation.

In summary, our findings appear robust to known sources of random and systematic error, but we acknowledge the possibility that unknown systematic uncertainties in the stellar mass determination may contribute to the difference in size–mass relations presented in our work. Future deep infrared spectroscopy may allow a more detailed investigation of the inherent uncertainties in determining stellar masses from photometric data.

4.3 A comparison with UVJ selection

To allow a comparison of our supercolour technique with previous work, in Figure 7 (left) we present a rest-frame UVJ colour-colour diagram for UDS galaxies in the redshift range $1 < z < 2$. As previously shown in W14, the classification of galaxies using supercolours agrees very well with the more traditional UVJ colour selection (Labbé et al. 2005; Wuyts et al. 2007). Post-starburst galaxies are generally found at the blue end of the passive UVJ region, in good agreement with the findings of Whitaker et al. (2012). The distribution in $U - V$ alone confirms that PSBs predominantly lie in the classic “green valley”, intermediate between passive and star-forming galaxies, but the addition of the $V - J$ colour isolates this population in the distinct region corresponding to the youngest red-sequence galaxies.

In the right-hand panel of Figure 7 we illustrate the average effective radii in colour-colour bins. We select the subset of galaxies over the mass range $10.5 < \log (M_*/M_\odot) < 11.5$ to minimise the

effects of the size–mass relation. The trends confirm that “young quiescent” galaxies selected by the UVJ technique show smaller average sizes, in good agreement with our analysis based on supercolours. Our results are consistent with a similar recent analysis by Yano et al. (2016).

5 THE SÉRSIC INDICES OF POST-STARBURST GALAXIES

In Figure 8 we compare the Sérsic indices for star-forming, passive and post-starburst galaxies at $z > 1$. The distributions obtained from the ground-based K -band data are consistent with those obtained for the smaller CANDELS sample. In both cases, we find that star-forming galaxies show a distribution peaking sharply at $n \approx 1$, while passive and post-starburst galaxies show very different distributions, peaking at significantly higher values. A Kolmogorov-Smirnov test confirms these findings, rejecting the null hypothesis that either passive or post-starburst galaxies are drawn from the same distribution as star-forming galaxies to a high level of significance ($>> 99.99\%$, using the ground-based sample). In contrast, the Sérsic distributions for passive and post-starburst galaxies do not appear significantly different.

The right-hand panel in Figure 8 presents the median Sérsic indices as a function of stellar mass. We find evidence for a slight increase in the median Sérsic index with stellar mass for all populations, but in all mass bins the post-starburst galaxies show significantly higher Sérsic indices than star-forming galaxies, and values consistent with the passive population. Using the mean produced very similar trends, but Sérsic indices were slightly higher in all cases (by $\delta n \approx 0.5$).

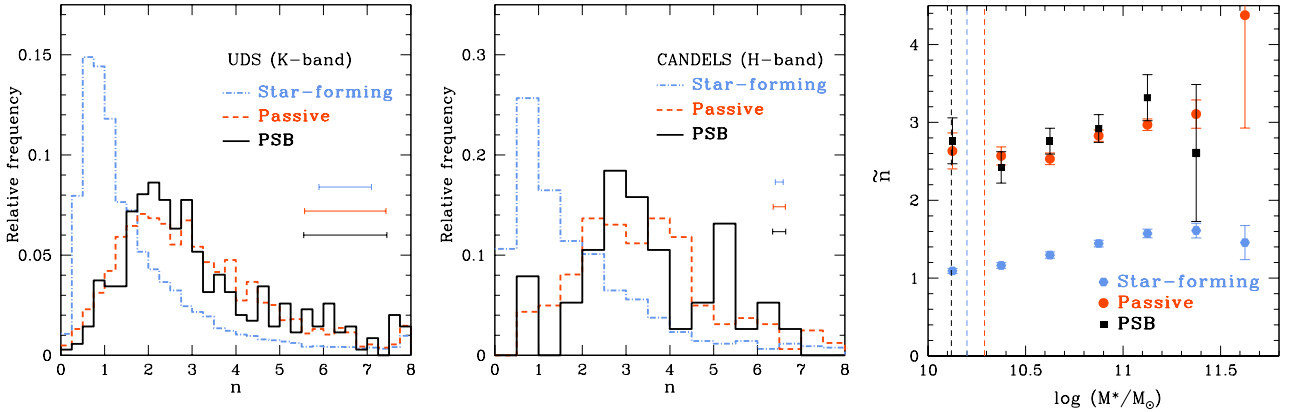


Figure 8. A comparison of the Sérsic indices for star-forming, passive and post-starburst galaxies in the redshift range $1 < z < 2$ with stellar masses $M_* > 10^{10} M_\odot$. The left panel shows a histogram of Sérsic indices determined from ground-based UDS K -band imaging. The central panel shows a histogram of Sérsic indices determined for the smaller sample with available HST H -band imaging from CANDELS (from van der Wel et al. 2012). Characteristic uncertainties are displayed for each population, showing the median error on the fitted Sérsic index for individual galaxies. The right panel shows median Sérsic indices as a function of stellar mass for the larger K -band sample, using identical binning to Figure 4. We conclude that post-starburst galaxies show significantly higher Sérsic indices than star-forming galaxies, but with a distribution that is indistinguishable from the older passive population.

We caution that single Sérsic fits provide only a crude parameterisation of the data, as it is now well-established that most galaxies at this epoch have more complex morphologies (e.g. Bruce et al. 2014). A high Sérsic index does not necessarily imply a purely spheroidal system, and low Sérsic indices do not necessarily imply the presence of an established disc (Mortlock et al. 2013). Nevertheless, it is clear from our data that the post-starburst galaxies are structurally very different to the actively star-forming population, and more comparable to ultra-compact equivalents of the passive population. We explore multiple-component fitting in future work (Maltby et al., in preparation).

6 DISCUSSION

We have presented evidence that massive ($M_* > 10^{10.5} M_\odot$) recently-quenched (post-starburst) galaxies at high redshift ($z > 1$) are exceptionally compact. Furthermore, they show high Sérsic indices, indistinguishable from the established passive population at the same epoch. We conclude that the structural transformation must have occurred before (or during) the event that quenched their star formation. Given that the majority of massive passive galaxies at $z > 1$ are thought to have passed through a post-starburst phase (Wild et al. 2016), our findings suggest a strong link between quenching and the formation of a compact spheroid.

Our results confirm the findings of Whitaker (2012), who found evidence that younger passive galaxies are more compact at $z > 1$, and the more recent HST CANDELS study by Yano et al. (2016). At intermediate redshifts ($z \sim 1$) previous studies have found conflicting results on the relationship between stellar age and the compactness of passive galaxies, with indications that progenitor bias may be playing a role at this epoch (Keating et al. 2015; Williams et al. 2017).

Our findings may be explained if high-redshift post-starburst galaxies are formed from the dramatic collapse of gas at high redshift, formed from either a gas-rich merger (e.g. Hopkins et al. 2009; Wellons et al. 2015), or from gas inflow feeding a massive disc, which becomes unstable and collapses by “compaction” (e.g. Dekel et al. 2009; Zolotov et al. 2015; Tacchella et al. 2016). Star

formation must then be rapidly quenched, either by a central AGN or feedback from highly nucleated star formation (e.g. Hopkins et al. 2005; Diamond-Stanic et al. 2012), leaving an ultra-compact post-starburst remnant. It may be possible to test these evolutionary scenarios by comparing the properties of post-starburst galaxies with their likely active progenitors, i.e. star-forming galaxies caught during the merging or “compaction” phase. Current candidates include submillimetre galaxies, many of which appear to be highly compact at $\sim 250 \mu\text{m}$ in the rest-frame (e.g. Simpson et al. 2015), and the high-redshift “blue nuggets” (e.g. Barro et al. 2013; Mei et al. 2015; Barro et al. 2017). Whatever the true progenitors for our PSBs, the most likely explanation is that structural transformation occurred immediately prior to quenching. The fact that the PSBs and passive galaxies have indistinguishable Sérsic indices (Figure 8) would suggest that most of the structural change is already established when the star formation is quenched, unless the structural transformation occurs on a much shorter timescale than the ~ 500 Myr lifetime for the PSB phase.

Following the formation of the proto-spheroid, there are currently two leading explanations for the observed growth in passive galaxies with cosmic time. Minor gas-free mergers provide a plausible physical mechanism (e.g. Bezanson et al. 2009; Naab, Johansson & Ostriker 2009), and indeed there is evidence that high-redshift passive galaxies are larger in dense environments, where such interactions are more likely (e.g. Lani et al. 2013). Alternatively, progenitor bias may mimic the observed growth, since passive galaxies formed at later times are typically larger (e.g. Poggianti et al. 2013; Carollo et al. 2013).

Our finding that post-starburst galaxies are more compact than older passive galaxies, on average, would suggest that we are observing an earlier phase in the lifetime of steadily-growing spheroids. Thus progenitor bias is unlikely to be the primary cause for the observed growth at early times; our observed trends show precisely the opposite behaviour (with younger galaxies being more compact). On the other hand, if massive post-starburst galaxies represent newly-formed “red nuggets”, it is notable that their abundance is a strong function of redshift; massive ($M_* > 10^{10.5} M_\odot$) post-starburst galaxies are several times more abundant at $z \sim 2$ compared to $z \sim 0.5$ (Wild et al. 2016). Thus, while the majority of high-mass

passive galaxies at $z \sim 2$ are likely to have been through the ultra-compact post-starburst phase (Wild et al. 2016), this may become an increasingly less dominant channel towards lower redshifts, when progenitor bias may play a more significant role in explaining size evolution (e.g. see Fagioli et al. 2016, Williams et al. 2017). Even at low redshift, however, there is evidence that the most compact quiescent galaxies have evolved from post-starburst progenitors (Zahid et al. 2016).

Finally, we note that the mass function for PSBs shows a very distinctive evolution in shape (Wild et al. 2016). At high redshift ($z \sim 2$) the mass function resembles that of quiescent galaxies, dominated by high-mass systems with a sharp decline in space density above a mass of $M_* \sim 10^{10.5} M_\odot$. At low redshift ($z < 1$) the population is dominated by lower-mass systems, with a shape resembling the mass function for star-forming galaxies. These features are interpreted as evidence for two distinct formation channels for post-starburst galaxies; high-mass systems formed from gas-rich dissipative collapse, and low-mass systems formed from environmental quenching or the merging of normal disc galaxies (Wild et al. 2016). Our structural findings are in good agreement with this scenario, with the PSBs above the same characteristic mass displaying distinctive, ultra-compact morphologies, consistent with a highly-dissipative, gas-rich origin. We will present a detailed study of the structural parameters for low-mass PSBs in future work (Maltby et al., in preparation).

7 CONCLUSIONS

We present a study of the structural parameters for a large sample of photometrically-selected post-starburst galaxies in the redshift range $1 < z < 2$, recently identified in the UKIDSS UDS field. These rare transition objects provide the ideal sample for understanding the links between the quenching of star formation and the structural transformation of massive galaxies.

We demonstrate that deep ground-based near-infrared imaging can be used to obtain robust sizes and Sérsic indices for large samples of high-redshift galaxies. From the resulting size–mass relation, we find that massive ($M_* > 10^{10.5} M_\odot$) post-starburst galaxies are exceptionally compact at $z > 1$, with evidence that they are more compact on average than established passive galaxies at the same epoch. Since most high-mass passive galaxies at $z > 1$ are likely to have been through a post-starburst phase (Wild et al. 2016), the implication is that quiescent galaxies are most compact when they are newly quenched, thereafter growing with cosmic time. An important caveat, however, is to acknowledge the considerable uncertainty in stellar mass estimation, as discussed in Section 4.2. As an avenue for future research, it will be important to determine whether stellar masses are systematically overestimated for recently quenched stellar populations.

We also find that post-starburst galaxies show high Sérsic indices, significantly higher than star-forming galaxies on average, but statistically indistinguishable from the Sérsic indices of established passive galaxies at the same epoch. We conclude that massive post-starburst galaxies represent newly-formed compact proto-spheroids. Furthermore, the structural transformation of these galaxies must have occurred before (or during) the event that quenched their star formation.

ACKNOWLEDGEMENTS

We thank Louis Abramson, Steven Bamford, Dale Kocevski, Mike Merrifield, and Ian Smail for useful discussions. We extend our gratitude to the staff at UKIRT for their tireless efforts in ensuring the success of the UDS project. We also wish to recognize and acknowledge the very significant cultural role and reverence that the summit of Mauna Kea has within the indigenous Hawaiian community. We were most fortunate to have the opportunity to conduct observations from this mountain. V.W. and K.R. and acknowledge support from the European Research Council Starting Grant (PI Wild). RJM acknowledges the support of the European Research Council via the award of a consolidator grant (PI McLure).

REFERENCES

- Barro G., et al., 2013, *ApJ*, 765, 104
 Barro G., et al., 2017, *ApJ*, 840, 47
 Barden M., Häußler B., Peng C. Y., McIntosh D. H., Guo Y., 2012, *MNRAS*, 422, 449
 Behroozi P. S., Conroy C., Wechsler R. H., 2010, *ApJ*, 717, 379
 Belli S., Newman A. B., Ellis R. S., Konidaris N. P., 2014, *ApJ*, 788, L29
 Best P. N., Kaiser C. R., Heckman T. M., Kauffmann G., 2006, *MNRAS*, 368, L67
 Bezanson R., van Dokkum P. G., Tal T., Marchesini D., Kriek M., Franx M., Coppi P., 2009, *ApJ*, 697, 1290
 Bruce V. A., et al., 2014, *MNRAS*, 444, 1001
 Bruzual G., Charlot S., 2003, *MNRAS*, 344, 1000
 Carollo C. M., et al., 2013, *ApJ*, 773, 112
 Casali M., et al., 2007, *A&A*, 467, 777
 Cirasuolo M., McLure R. J., Dunlop J. S., Almaini O., Foucaud S., Simpson C., 2010, *MNRAS*, 401, 1166
 Daddi E., et al., 2005, *ApJ*, 626, 680
 Dekel A., et al., 2009, *Nature*, 457, 451
 Diamond-Stanic A. M., Moustakas J., Tremonti C. A., Coil A. L., Hickox R. C., Robaina A. R., Rudnick G. H., Sell P. H., 2012, *ApJ*, 755, L26
 Dressler A., Gunn J. E., 1983, *ApJ*, 270, 7
 Fagioli M., Carollo C. M., Renzini A., Lilly S. J., Onodera M., Tacchella S., 2016, *ApJ*, 831, 173
 Fan L., Lapi A., De Zotti G., Danese L., 2008, *ApJ*, 689, L101
 Fontana A., et al., 2004, *A&A*, 424, 23
 Furusawa H., et al., 2008, *ApJS*, 176, 1
 Gallazzi A., Charlot S., Brinchmann J., White S. D. M., 2006, *MNRAS*, 370, 1106
 Grogin N. A., et al., 2011, *ApJS*, 197, 35
 Hartley W. G., et al., 2013, *MNRAS*, 431, 3045
 Hogg D. W., et al., 2002, *AJ*, 124, 646
 Hopkins P. F., 2012, *MNRAS*, 420, L8
 Hopkins P. F., Hernquist L., Cox T. J., Di Matteo T., Martini P., Robertson B., Springel V., 2005, *ApJ*, 630, 705
 Hopkins P. F., Hernquist L., Cox T. J., Keres D., Wuyts S., 2009, *ApJ*, 691, 1424
 Keating S. K., Abraham R. G., Schiavon R., Graves G., Damjanov I., Yan R., Newman J., Simard L., 2015, *ApJ*, 798, 26
 Kelvin L. S., et al., 2012, *MNRAS*, 421, 1007
 Khochfar S., Silk J., 2009, *MNRAS*, 397, 506
 Kodama T., et al., 2004, *MNRAS*, 350, 1005
 Koekemoer A. M., et al., 2011, *ApJS*, 197, 36
 Labbé I., et al., 2005, *ApJ*, 624, L81
 Lani C., et al., 2013, *MNRAS*, 435, 207
 Lawrence A., et al., 2007, *MNRAS*, 379, 1599
 Maltby D. T., et al., 2016, *MNRAS*, 459, L114
 Maraston C., Daddi E., Renzini A., Cimatti A., Dickinson M., Papovich C., Pasquali A., Pirzkal N., 2006, *ApJ*, 652, 85
 Mei S., et al., 2015, *ApJ*, 804, 117
 McLure R. J., et al., 2013, *MNRAS*, 428, 1088

- Mortlock A., et al., 2013, MNRAS, 433, 1185
Muzzin A., Marchesini D., van Dokkum P. G., Labb
Naab T., Johansson P. H., Ostriker J. P., 2009, ApJ, 699, L178
Peng C. Y., Ho L. C., Impey C. D., Rix H.-W., 2002, AJ, 124, 266
Poggianti B. M., et al., 2013, ApJ, 762, 77
Pozzetti L., et al., 2010, A&A, 523, A13
Sersic J. L., 1968, adga.book,
Silk J., Rees M. J., 1998, A&A, 331, L1
Simpson C., Westoby P., Arumugam V., Ivison R., Hartley W., Almaini O.,
2013, MNRAS, 433, 2647
Simpson J. M., et al., 2015, ApJ, 799, 81
Straatman C. M. S., et al., 2015, ApJ, 808, L29
Strateva I., et al., 2001, AJ, 122, 1861
Tacchella S., Dekel A., Carollo C. M., Ceverino D., DeGraf C., Lapiner S.,
Mandelker N., Primack J. R., 2016, MNRAS, 458, 242
Trujillo I., et al., 2006, MNRAS, 373, L36
van der Wel A., et al., 2012, ApJS, 203, 24
van der Wel A., et al., 2014, ApJ, 788, 28
van Dokkum P. G., et al., 2008, ApJ, 677, L5
van Dokkum P. G., et al., 2015, ApJ, 813, 23
Vergani D., et al., 2010, A&A, 509, A42
Wellons S., et al., 2015, MNRAS, 449, 361
Whitaker K. E., Kriek M., van Dokkum P. G., Bezanson R., Brammer G.,
Franx M., Labbé I., 2012, ApJ, 745, 179
Wild V., Walcher C. J., Johansson P. H., Tresse L., Charlot S., Pollo A., Le
Fèvre O., de Ravel L., 2009, MNRAS, 395, 144
Wild V., et al., 2014, MNRAS, 440, 1880
Wild V., Almaini O., Dunlop J., Simpson C., Rowlands K., Bowler R.,
Maltby D., McLure R., 2016, MNRAS, 463, 832
Williams C. C., et al., 2017, ApJ, 838, 94
Wuyts S., et al., 2007, ApJ, 655, 51
Yano M., Kriek M., van der Wel A., Whitaker K. E., 2016, ApJ, 817, L21
Zahid H. J., Baeza Hochmuth N., Geller M. J., Damjanov I., Chilingarian
I. V., Sohn J., Salmi F., Hwang H. S., 2016, ApJ, 831, 146
Zolotov A., et al., 2015, MNRAS, 450, 2327

APPENDIX A: ROBUSTNESS TESTS

In this section we discuss a number of additional tests that were performed to investigate the robustness of the size–mass relations presented in this paper.

Throughout this work we have measured average sizes when comparing galaxy populations, yielding evidence that post-starburst galaxies are typically smaller than passive galaxies of comparable stellar mass. The use of a mean may produce misleading results, however, if either population is skewed by a significant number of outliers (e.g. misclassified interlopers from other galaxy categories). In Figure A1 (left panel) we therefore reproduce the size–mass relation from Figure 4, but this time using median size values. In most bins the median sizes are slightly smaller than the mean, as the size distributions show a slight tail to high values. The significant differences between the passive and post-starburst galaxies remain, however. At high-mass ($M_* > 10^{10.5} M_\odot$) the overall significance of the trends is essentially unchanged compared to the results outlined in Section 4.1. We conclude that the use of a mean has not biased our primary conclusions.

As a further source of error, we considered the possibility that the passive and post-starburst samples are contaminated by star-forming galaxies, e.g. due to uncertainties in classification. If the contaminating fraction is higher for the passive population (for reasons unknown), this could skew the size measurements upwards. We tested for this effect by applying a cut in Sérsic index. Noting the very different distributions in Sérsic index between star-forming and passive samples (see Figure 8), we re-evaluated the size–mass

relations using only passive and post-starburst galaxies with $n > 2$ (see Figure A1, right panel), again using the median size to further reduce the impact of interlopers. The striking difference in sizes remains, with a negligible reduction in significance. Using a mean estimator yields the same result, with a size–mass relation that is almost identical to the upper-right panel of Figure 4. We conclude that “contamination” from galaxies with low Sérsic indices (whether passive or star-forming) is not affecting our conclusions.

As an additional test, we investigated the influence of using a cleaner (though less complete) sample of post-starburst galaxies. As outlined in Section 1 and Maltby et al. (2016), the primary source of contamination is between post-starburst galaxies and “normal” passive galaxies. Depending on the precise selection criteria, between 20–40% galaxies in the PSB category would be classified as passive (rather than PSB) using spectroscopy, while 6–10% of the passive category would be spectroscopically classified as PSBs (Maltby; private communication). Based on Figure 3 in Maltby et al. (2016), we therefore identify a “cleaner” PSB sample by selecting galaxies further from the passive/PSB boundary, with supercolours $SC2 > 6$. In this regime, formally 100% of PSB candidates (15/15) were confirmed with $W_{H\delta} > 5\text{Å}$. Using this new sub-sample, the resulting size–mass relation (evaluated using the standard mean estimator) is shown in Figure A2 (left panel). We find that the difference in size compared to passive galaxies remains, and in fact is slightly enhanced; the mean PSB size is formally smaller in five out of six bins. We conclude that contamination of the PSB category by older passive galaxies can only act to dilute the differences we observe.

As another test for contamination, we combined the PCA classification with the classic UVJ criteria (e.g. see Figure 7), to exclude PSBs and passive galaxies that are classified as “star-forming” using rest-frame UVJ colours. The aim is to remove red star-forming galaxies that may have been misclassified by the PCA technique. Using these joint criteria removes 26% of passive galaxies and 34% of PSBs from our primary sample ($z > 1$, $M_* > 10^{10} M_\odot$). The resulting size–mass relations are shown in Figure A2 (right panel). We find that the difference between the PSBs and passive galaxies at high mass remains, and in fact is slightly enhanced.

Finally, we performed a variety of tests using more stringent cuts on the structural parameters derived for our ground-based galaxy sample, using the CANDELS dataset as a calibrating sample. No significant differences were found. We noted, however, that ground-based size measurements become increasingly unreliable when GALFIT assigns a very low axis ratio, $q < 0.1$. Approximately 6% of the galaxies in our sample are affected, mostly among the star-forming galaxies, but also affecting 3–4% of the passive and post-starburst sample (mostly at low mass; $M_* < 10^{10.5} M_\odot$). Removing these galaxies had no major influence on the size–mass relations; in fact, the difference in size between passive and post-starburst galaxies became marginally more significant.

This paper has been typeset from a $\text{\TeX}/\text{\LaTeX}$ file prepared by the author.

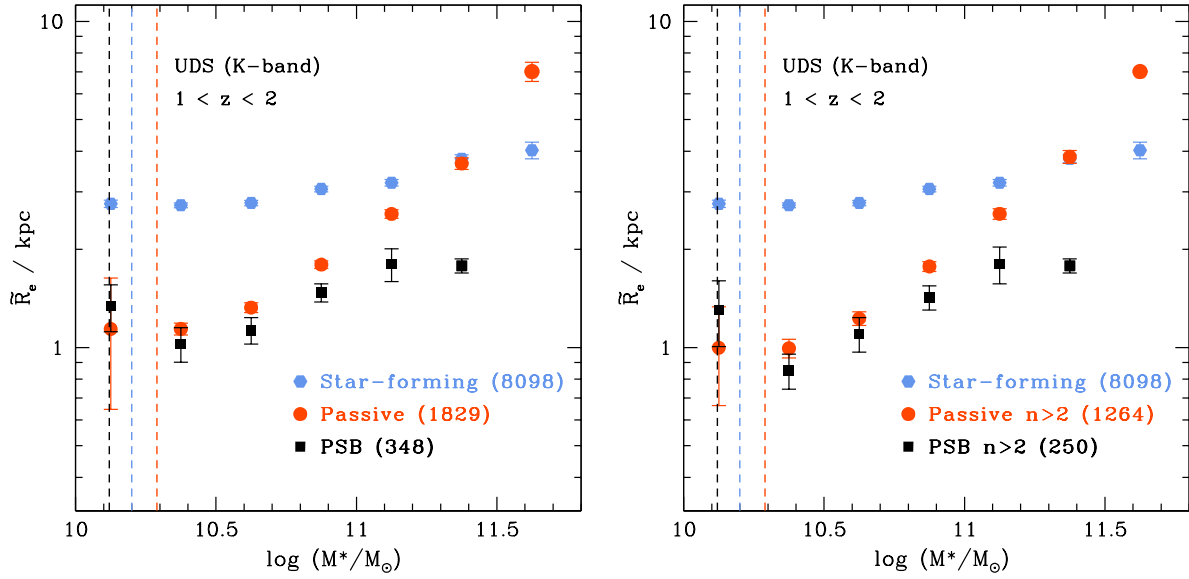


Figure A1. Two examples of tests for robustness. The left panel shows the size–mass relation for comparison with Figure 4 ($1 < z < 2$), but using the median rather than the mean effective radius per bin. The right panel shows the size–mass relation (also using median values) after the removal of all passive and post-starburst galaxies with $n < 2$. Since star-forming galaxies have significantly lower Sérsic indices (see Figure 8), this is a test to determine if contamination from SF galaxies is affecting the size–mass relations. In both cases, we find that our primary conclusions are unchanged, i.e. post-starburst galaxies at high mass ($M_* > 10^{10.5} M_\odot$) appear significantly smaller than both star-forming and passive galaxies.

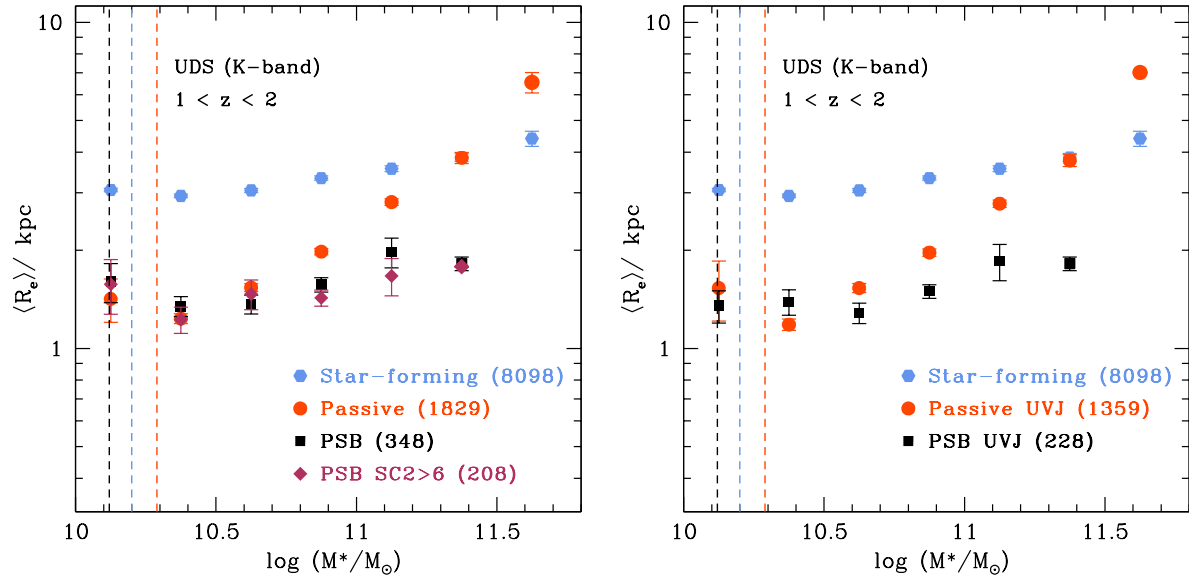


Figure A2. Two further tests for robustness. The left panel shows the ground-based size–mass relation, using the mean size (as shown in Figure 4), with the addition of a comparison sample of “secure” PSBs, identified further from the passive/PSB boundary (with supercolours $SC2 > 6$). The right panel shows the size–mass relation using only the subset of passive galaxies and PSBs that simultaneously lie within the quiescent region of the UVJ diagram (e.g. see Figure 7). In both cases, we find little change in the observed trends, with evidence for a slight enhancement in the difference between high mass PSBs and passive galaxies using the restricted samples.